

# Visualizing the Underlying Signaling Pathway Related to Nitric Oxide and Glutathione in Cardiovascular Disease Therapy by a Sequentially Activated Fluorescent Probe

Xiao-Xiao Chen, Li-Ya Niu,\* and Qing-Zheng Yang\*



Cite This: *Anal. Chem.* 2021, 93, 3922–3928



Read Online

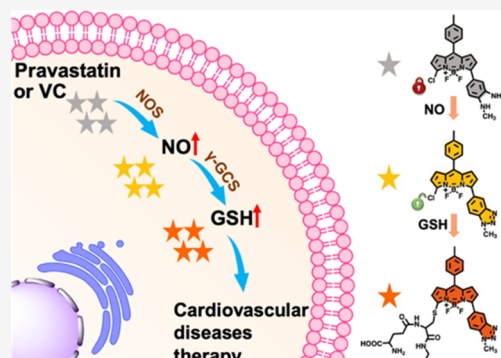
ACCESS |

Metrics & More

Article Recommendations

Supporting Information

**ABSTRACT:** Clarifying the signaling pathway associated with nitric oxide (NO) and glutathione (GSH) in cardiovascular disease therapy is important for understanding its physiological and pathological processes but is challenging due to the lack of efficient analytical techniques. Herein, we report a BODIPY-based fluorescent probe for recognition of NO and GSH in sequence with high sensitivity and selectivity. The probe exhibits turn-on fluorescence triggered by NO, followed by red-shifted emission in the presence of GSH. The sequentially activated mechanism allows the visualization of NO-induced GSH upregulation in drug-treated endothelial cells and zebrafish for the first time, revealing a signal pathway during the therapy. We hope that it can be used as a convenient and efficient tool for the study of the interplay between NO and GSH and for the screening of effective drugs for cardiovascular disease therapy.



Cardiovascular diseases, such as thrombosis, atherosclerosis, and heart failure, have been recognized as a major cause of death and disability around the world. Endothelial cells are the gatekeeper of cardiovascular homeostasis because they make a special barrier that selectively limits macromolecules moving between the bloodstream and blood vessel wall.<sup>1</sup> Evidence suggests that oxidative stress contributes to endothelial dysfunction considerably and afterward proceeds the progression of cardiovascular diseases.<sup>2</sup> Effective drugs like pravastatin and vitamin C (VC) have been used for the prevention and therapy of cardiovascular diseases in clinics.<sup>3,4</sup> To clarify how drugs work in the complex signaling pathway, researchers are mainly focusing on biomacromolecules using conventional biological methods, including western blotting analysis,<sup>5</sup> enzyme immunoassay kit,<sup>6</sup> and polymerase chain reaction (PCR) assay.<sup>7</sup> By comparison, the study of endogenously produced active small molecules remains underexplored, although they act as another important factor during therapies. Nitric oxide (NO), synthesized by NO synthase (NOS), possesses cardioprotective effects by inducing vasodilation, preventing platelet aggregation and cell adhesion, inhibiting the proliferation of smooth muscle cells, as well as disrupting the expression of proinflammatory genes.<sup>8</sup> On the other hand, glutathione (GSH) can maintain the cellular redox homeostasis via defending against oxidative stress, which may be beneficial to cardiovascular disease therapy. However, there is still a lack of direct evidence to reveal the connection between them during the treatment. The traditional methods for analysis of NO and GSH are chromatographic techniques and mass analyses, which require sample pretreatment

procedures to isolate the analytes from their native environments. These limitations hamper the direct observation of NO and GSH during cardiovascular disease therapy. Therefore, a suitable method is urgently needed to monitor their potential correlation *in vivo*, which is especially helpful to explain how signaling networks are regulated from a molecular level and to shed light on potential drug targets.

Fluorescent probes provide an opportunity for real-time and *in situ* monitoring of interactions of NO and GSH due to nondestructive detection and high sensitivity with spatiotemporal dynamic information.<sup>9–14</sup> To date, a great number of fluorescent probes have been developed for the detection of NO<sup>15–24</sup> or GSH<sup>25–34</sup> separately. The utilization of two different fluorescent probes to evaluate the possible correlation between NO and GSH in a biological system is inaccurate and complicated because each individual probe possesses different localizations, various cellular uptake mechanisms, and potential cross talks.<sup>35–39</sup> To develop a single fluorescent probe for simultaneous detection of NO and GSH is promising to solve these problems but is challenging due to the difference in lifetimes of NO and GSH under physiological conditions. Herein, we report a sequentially activated fluorescent probe 1

Received: November 11, 2020

Accepted: February 2, 2021

Published: February 15, 2021



ACS Publications

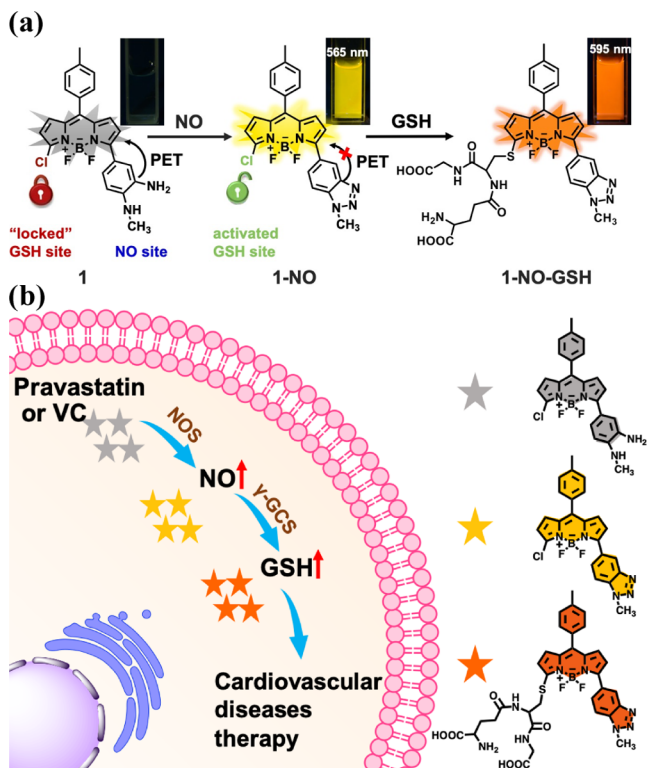
© 2021 American Chemical Society

3922

<https://dx.doi.org/10.1021/acs.analchem.0c04754>  
*Anal. Chem.* 2021, 93, 3922–3928

for imaging the interplay of NO and GSH from distinct emission channels in living cells and zebrafish (Scheme 1). The

**Scheme 1. (a) Proposed Mechanism of 1 for the Detection of NO and GSH and (b) Schematic Illustration of Cardiovascular Disease Therapy Accompanied by Sequential Generation of NO and GSH Monitored by 1 in Human Umbilical Vein Endothelial Cells (HUVECs)**



probe displayed enhanced yellow emission through NO-mediated transformation of diamine into a triazole, followed by a GSH-induced S<sub>N</sub>Ar substitution reaction to induce a red shift of fluorescence. It has been successfully used to visualize an endogenous burst of NO, which further induces GSH upregulation elicited by pravastatin or VC, revealing a signaling pathway during cardiovascular disease therapy. To our best knowledge, it is the first example of visualizing the NO-induced GSH upregulation during cardiovascular disease therapy both *in vitro* and *in vivo*.

## EXPERIMENTAL SECTION

**General Methods and Information.** All of the reagents and solvents were purchased from commercial suppliers (Beijing Chemical Works and Beijing Innochem Science & Technology Co., Ltd.) and used without further purification. <sup>1</sup>H and <sup>13</sup>C nuclear magnetic resonance (NMR) spectra were obtained on an Advance Bruker spectrometer or a JEOL spectrometer. Mass spectra were obtained on a Thermo Fisher Q-Exactive or Bruker Solarix XR Fourier Transform Ion Cyclotron Resonance Mass Spectrometer. Fluorescence spectra were recorded on a Hitachi 4500 spectrophotometer. Absorption spectra were recorded on a Shimadzu UV-1601PC UV-visible spectrophotometer. The cell viability test was obtained on a Thermo Scientific Multiskan. Confocal fluorescence imaging was performed with a Nikon A1R confocal microscope with a 60× oil-immersion objective lens.

Emission was collected at 555–570 nm for the yellow channel and at 590–605 nm for the red channel (excited at 487 nm).

**Preparation of the Test Solution.** We prepared a stock solution of 1 (1.0 mM) in acetonitrile (CH<sub>3</sub>CN). The stock solution of 1 was diluted to the corresponding concentration (10 μM) with CH<sub>3</sub>CN/phosphate-buffered saline (PBS) buffer (1:3 v/v, 1 mM, pH 7.4). Fresh DEA·NONOate (200 μM) solutions were prepared in 0.01 mM NaOH. The solution of GSH (200 μM) was freshly prepared in deionized water. N-Ethylmaleimide (NEM, 1.0 mM) solutions were prepared in dimethyl sulfoxide (DMSO). Pravastatin, VC, L-buthionine-sulfoximine (BSO), and L-NAME were dissolved in deionized water.

**Determination of the Detection Limit.** The detection limit was calculated based on the fluorescence titration method. The fluorescence emission spectra of 1 were detected six times, and the standard deviation of blank measurement was achieved. To obtain the value for the slope, the fluorescence intensity at 565 nm was plotted as a concentration of DEA·NONOate. The detection limit was calculated by detection limit  $3\sigma/k$ , where  $\sigma$  is the standard deviation of six blank measurements and  $k$  is the slope between the fluorescence intensity and DEA·NONOate concentration.

**Cell Counting Kit-8 Assay.** The Cell Counting Kit-8 (CCK-8) cell proliferation assay was applied to investigate the cytotoxicity of 1. Cells were seeded into a 96-well plate and incubated with 100 μL of Dulbecco's modified Eagle's medium (DMEM). After 24 h of cell attachment, the plates were washed with PBS, followed by the addition of increasing concentrations of probe 1 (0.5–16 μM) in DMEM. The cells were then incubated at 37 °C in an atmosphere of 5% CO<sub>2</sub> and 95% air for 12 h, followed by standard CCK-8 assays ( $n = 6$ ). Untreated assays ( $n = 6$ ) were also conducted under the same conditions. The absorbance at 450 nm was measured by the Thermo Scientific Multiskan. Cell viability (%) =  $(A_{\text{with probe}} - A_{\text{blank}}/A_{\text{control}} - A_{\text{blank}}) \times 100\%$ .

**Cell Culture.** HUVECs were grown in DMEM supplemented with 10% fetal bovine serum (FBS) at 37 °C in a humidified environment of 5% CO<sub>2</sub>. Cells were plated on a glass-bottom cell culture dish (30 mm) and allowed to adhere for 12 h. Before confocal imaging, cells were washed with phosphate buffer saline (PBS) three times.

**Zebrafish Imaging.** Two-day-old zebrafish were grown in E3 embryo media (15 mM NaCl, 0.5 mM KCl, 1 mM MgSO<sub>4</sub>, 1 mM CaCl<sub>2</sub>, 0.15 mM KH<sub>2</sub>PO<sub>4</sub>, 0.05 mM Na<sub>2</sub>HPO<sub>4</sub>, 0.7 mM NaHCO<sub>3</sub>, 5–10% methylene blue; pH = 7.4) at 28 °C. Moreover, this embryo medium was supplemented with 1-phenyl-2-thiourea (PTU) to inhibit melanin formation in zebrafish. For exogenous NO and GSH imaging, the methods are similar to the preceding ways in HUVECs. For monitoring the NO and GSH concentration changes induced by pravastatin or VC, zebrafish were fed with pravastatin or VC (50.0 μM) for 24 h and then treated with 1 (2.0 μM) for 30 min. After removing the medium by washing with PBS three times, we image these zebrafish under a confocal microscope.

## RESULTS AND DISCUSSION

**Design and Synthesis of Probe 1.** We rationally designed probe 1 by combining an *o*-phenylenediamine (OPD) moiety at the 5-position of the BODIPY core as a NO-capturing indicator and chlorine at the 3-position as a GSH responsive site. As depicted in Scheme 1a, 1 is nonfluorescent due to photoinduced electron transfer

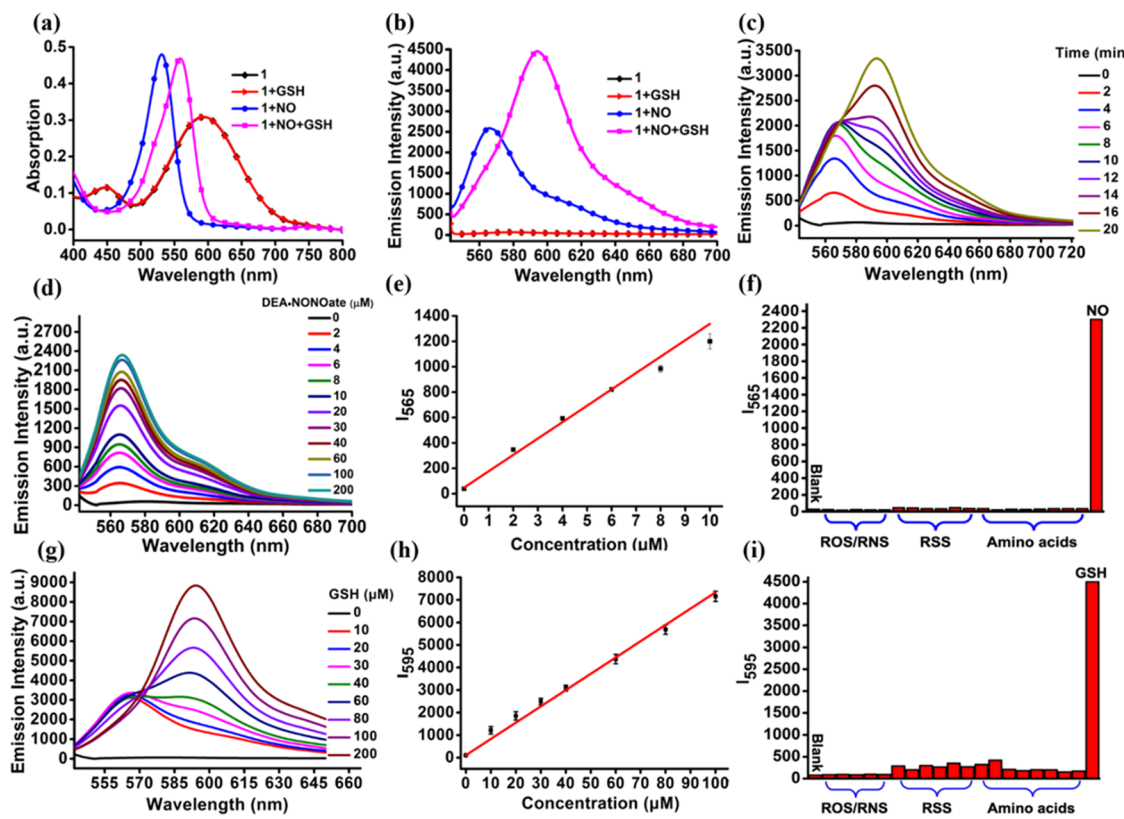


**Figure 1.** (a) Absorption spectra of **1** upon addition of DEA-NONOate (200  $\mu$ M) and GSH (200  $\mu$ M) for 2 h. (b) Fluorescence spectra of **1** upon addition of DEA-NONOate (200  $\mu$ M) and GSH (200  $\mu$ M) for 1 h. (c) Time-dependent fluorescence spectra of **1** (10  $\mu$ M) upon addition of DEA-NONOate (200  $\mu$ M) in the presence of GSH (200  $\mu$ M). (d) Fluorescence spectra of **1** (10  $\mu$ M) treated with DEA-NONOate (0–200  $\mu$ M) for 1 h. Slit: 2.5/2.5. (e) Corresponding linear relationship between the fluorescent intensity and DEA-NONOate concentration ( $R^2 = 0.993$ ). (f) Fluorescence intensities of **1** (10  $\mu$ M) upon addition of various species after 30 min. ROS/RNS:  $\text{NO}_3^-$  (200  $\mu$ M),  $\text{NO}_2^-$  (200  $\mu$ M),  $\text{O}_2$  (200  $\mu$ M),  $\cdot\text{OH}$  (200  $\mu$ M),  $\text{H}_2\text{O}_2$  (200  $\mu$ M); RSS:  $\text{HS}^-$  (1 mM),  $\text{SO}_4^{2-}$  (1 mM),  $\text{S}_2\text{O}_5^{2-}$  (1 mM),  $\text{HSO}_4^-$  (1 mM),  $\text{HSO}_3^-$  (1 mM),  $\text{SO}_3^{2-}$  (1 mM); amino acids: Cys (200  $\mu$ M), Hcy (20  $\mu$ M), His (1 mM), Iso (1 mM), Leu (1 mM), Lys (1 mM), Met (1 mM), Ser (1 mM), GSH (1 mM). (g) Fluorescence spectra of **1** (10  $\mu$ M) treated with increasing concentrations of GSH (0–200  $\mu$ M) in the presence of DEA-NONOate (200  $\mu$ M). Slit: 5.0/5.0. (h) Corresponding linear relationship between the fluorescent intensity and GSH concentrations ( $R^2 = 0.997$ ). (i) Fluorescence intensities of **1** (10  $\mu$ M) upon addition of 20 equiv of DEA-NONOate and various species simultaneously for 1 h. Blank: probe **1**; ROS/RNS:  $\text{NO}_3^-$  (200  $\mu$ M),  $\text{NO}_2^-$  (200  $\mu$ M),  $\text{O}_2$  (200  $\mu$ M),  $\cdot\text{OH}$  (200  $\mu$ M),  $\text{H}_2\text{O}_2$  (200  $\mu$ M); RSS:  $\text{HS}^-$  (1 mM),  $\text{SO}_4^{2-}$  (1 mM),  $\text{S}_2\text{O}_5^{2-}$  (1 mM),  $\text{HSO}_4^-$  (1 mM),  $\text{HSO}_3^-$  (1 mM),  $\text{SO}_3^{2-}$  (1 mM); amino acids: Cys (200  $\mu$ M), Hcy (20  $\mu$ M), His (1 mM), Iso (1 mM), Leu (1 mM), Lys (1 mM), Met (1 mM), Ser (1 mM), GSH (1 mM).  $\lambda_{\text{ex}} = 532$  nm.

(PET).<sup>15</sup> Initially, the chlorine at the 3-position exhibits no reactivity toward GSH because an electron-donating OPD group at the 5-position lowers the electrophilicity of the 3-position.<sup>40–42</sup> In the presence of NO, **1**-NO is generated through the transformation of diamine to triazole and shows significant fluorescence increase by inhibiting the PET process. At the same time, benzotriazole with electron-withdrawing ability activated the nucleophilic reactivity of the 3-position toward GSH. Consequently, the chlorine at the 3-position is replaced by GSH through an  $\text{S}_{\text{N}}\text{Ar}$  substitution reaction, resulting in the formation of **1**-NO-GSH with red-shifted fluorescence. In this regard, the interplay of NO and GSH can be monitored sequentially from two emission signals. Probe **1** was synthesized (Figure S1) and characterized by  $^1\text{H}$  and  $^{13}\text{C}$  NMR spectroscopy and high-resolution mass spectrometry (HRMS) (Figures S2–S4).

**Spectrographic Properties of Probe 1 toward NO and GSH.** To confirm our hypothesis, we investigated the spectroscopic properties of **1** for the detection of NO and GSH in a solution. As shown in Figure 1a,b, **1** intrinsically possessed a maximum absorption peak centered at 600 nm. The fluorescence of **1** is weak, which is ascribed to the PET

process (Figure 1b). Upon addition of DEA-NONOate, the maximum absorption peak of **1** blue-shifted from 600 to 532 nm, and the emission at 565 nm increased because the formation of **1**-NO blocked the PET process, which was confirmed by HRMS (Figure S5). The reaction of **1** with NO reached a plateau within 6 min, indicating that **1** is capable of efficient detection of NO (Figure S7a,b). After treating with GSH, there were no changes in the absorption spectra and no fluorescence recovery because of the low reactivity of chlorine at the 3-position of the BODIPY core with an electron-donating OPD at the 5-position. When **1** was treated with DEA-NONOate and GSH simultaneously, a new maximum absorption peak appeared at 562 nm, and the emission at 565 nm increased within 10 min, demonstrating **1**-NO formation (Figure 1c). Upon prolonging the incubation time to 1 h, the emission peak at 565 nm red-shifted to 595 nm gradually (Figure 1c), indicating the transformation of **1**-NO to **1**-NO-GSH. The formation of **1**-NO-GSH is further confirmed by HRMS (Figure S6). The formation of electron-withdrawing triazole activated the reactivity of chlorine toward GSH, allowing the sequential recognition of NO and GSH. The results proved that probe **1** only responds to GSH in the prior

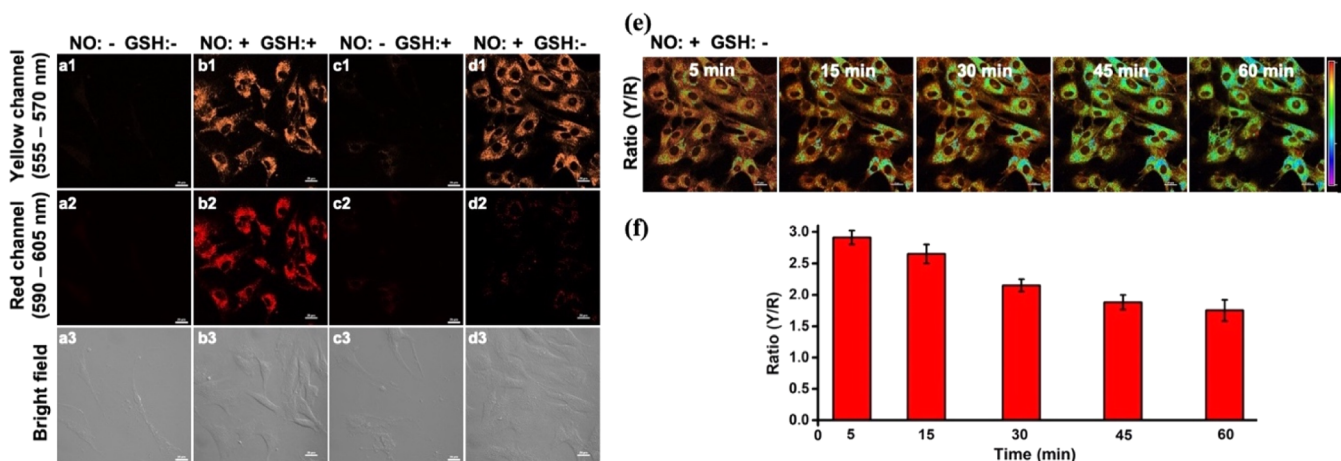


**Figure 2.** Fluorescence imaging of **1** (2  $\mu$ M, 5 min) in HUVECs: (a1–a3) pretreated with NEM (1 mM, 30 min), (b1–b3) pretreated with DEA-NONOate (200  $\mu$ M, 15 min), (c1–c3) non-pretreated, and (d1–d3) pretreated with NEM (1 mM, 30 min) and then DEA-NONOate (200  $\mu$ M, 15 min). (e) Real-time confocal imaging of HUVECs cultured by NEM (1 mM, 30 min), DEA-NONOate (200  $\mu$ M, 15 min), and then **1** (2  $\mu$ M, 5 min). (f) Fluorescence intensity ratios of the yellow to red channel in HUVECs. Emission was collected at 555–570 nm for the yellow channel and 590–605 nm for the red channel (excited at 487 nm). Scale bar: 20  $\mu$ m.

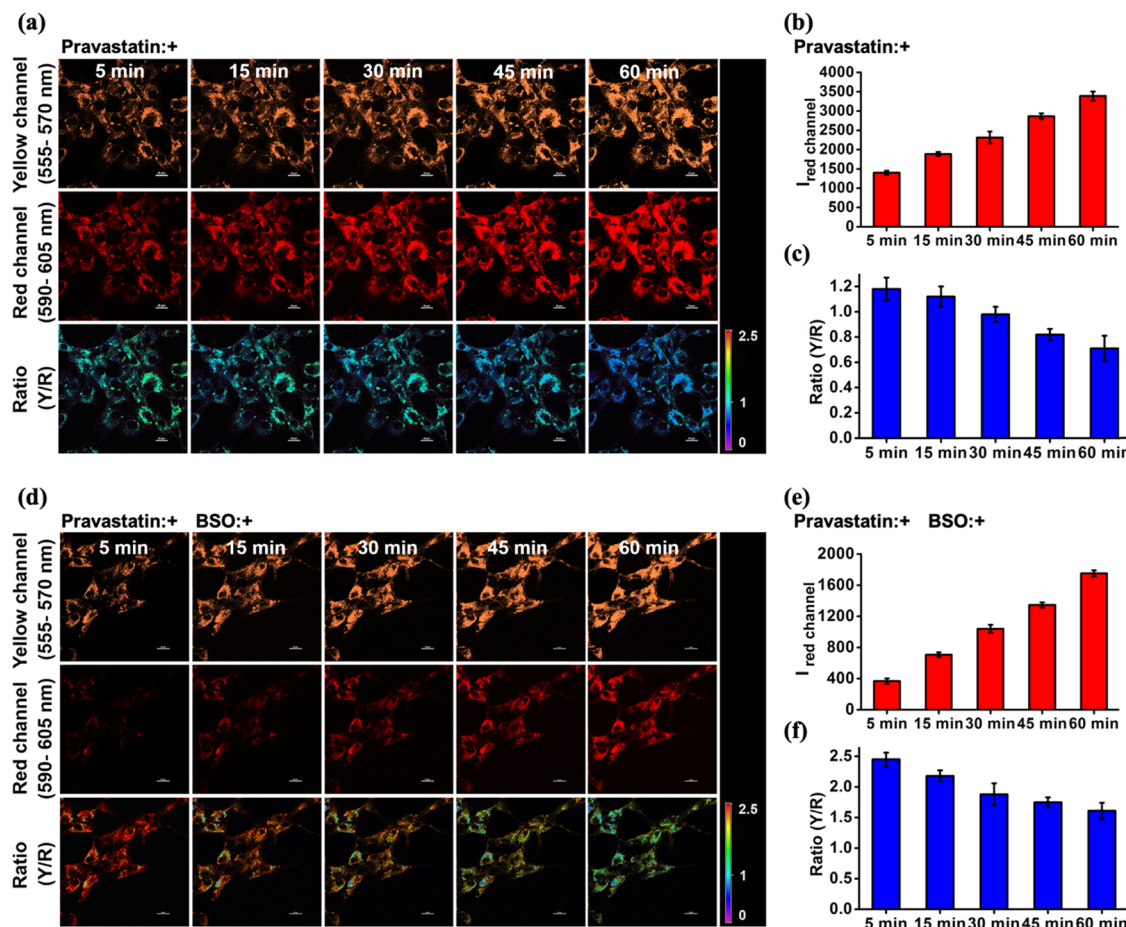


**Figure 3.** (a) Time-dependent confocal fluorescence imaging of HUVECs pretreated with pravastatin (0.5 mM, 12 h) and then cultured with **1** (2  $\mu$ M, 5 min). (b) Mean fluorescence intensity of the red channel (590–605 nm) at various times after incubation with pravastatin and **1**. (c) Average fluorescence intensity ratios (yellow/red) at different times after incubation with pravastatin and **1**. (d) Time-dependent confocal fluorescence imaging of HUVECs pretreated with pravastatin (0.5 mM, 12 h), further incubated with BSO (0.5 mM, 6 h) and then incubated with **1** (2  $\mu$ M, 5 min). (e) Mean fluorescence intensity of the red channel (590–605 nm) at various times after incubation with pravastatin, BSO, and **1**. (f) Average fluorescence intensity ratios (yellow/red) at different times after incubation with pravastatin, BSO, and **1**. Emission was collected at 555–570 nm for the yellow channel and 590–605 nm for the red channel (excited at 487 nm). Scale bar: 20  $\mu$ m.

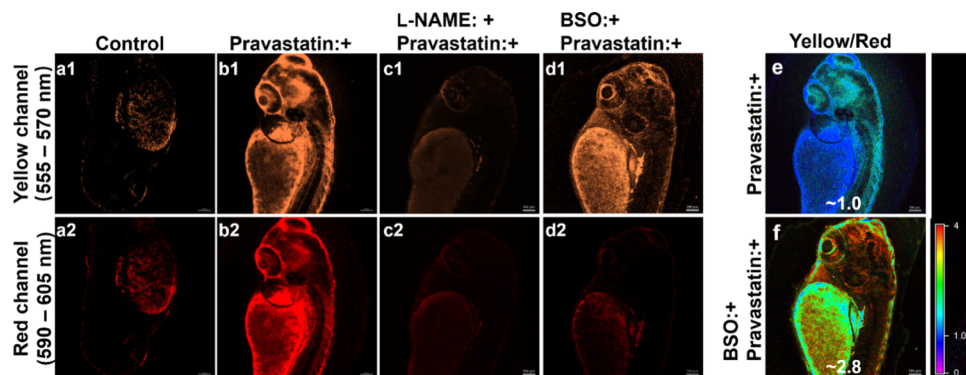


**Figure 4.** Fluorescence imaging of living zebrafish treated with **1** ( $2 \mu\text{M}$ , 30 min): (a1, a2) control image, (b1, b2) pretreated with pravastatin ( $50 \mu\text{M}$ , 24 h), (c1, c2) pretreated with pravastatin ( $50 \mu\text{M}$ , 24 h) and further incubated with L-NAME ( $100 \mu\text{M}$ , 12 h), and (d1, d2) pretreated with pravastatin ( $50 \mu\text{M}$ , 24 h) and further incubated with BSO ( $200 \mu\text{M}$ , 12 h). Emission was collected at  $555\text{--}570 \text{ nm}$  for the yellow channel and at  $590\text{--}605 \text{ nm}$  for the red channel (excited at  $487 \text{ nm}$ ). Ratiometric confocal fluorescence images (yellow/red channels): (e) zebrafish treated with pravastatin ( $50 \mu\text{M}$ , 24 h) and then **1** ( $2 \mu\text{M}$ , 30 min). (f) Zebrafish cultured by pravastatin ( $50 \mu\text{M}$ , 24 h), further incubated with BSO ( $200 \mu\text{M}$ , 12 h), and then **1** ( $2 \mu\text{M}$ , 30 min). Scale bar:  $100 \mu\text{m}$ .

presence of NO so that the red fluorescence can only be observed when there is a cross talk between NO and GSH. Moreover, in the presence of different concentrations of DEA-NONOate ( $0\text{--}200 \mu\text{M}$ ), there was a gradual increase in the emission peak at  $565 \text{ nm}$  with an excitation at  $532 \text{ nm}$  (Figure 1d). A linear functional relationship ( $R^2 = 0.993$ ) was obtained between the fluorescence intensity at  $565 \text{ nm}$  and the concentration of DEA-NONOate ranged from 0 to  $10 \mu\text{M}$  (Figure 1e). The detection limit ( $3\sigma/\text{slope}$ ) for NO was calculated to be  $3.4 \times 10^{-8} \text{ M}$ . Furthermore, no marked fluorescence enhancement of **1** in the presence of ROS/RNS, RSS, and different amino acids and active biotihols (Cys, Hcy) was observed, while the treatment of **1** with DEA-NONOate induced a large fluorescence enhancement at  $565 \text{ nm}$ , indicating that **1** possesses excellent selectivity with respect to NO (Figure 1f). As depicted in Figure 1g, when **1** was treated with both DEA-NONOate ( $200 \mu\text{M}$ ) and various concentrations of GSH ( $0\text{--}200 \mu\text{M}$ ), the fluorescence intensity at  $595 \text{ nm}$  exhibited a linear relationship against the GSH amount from 0 to  $100 \mu\text{M}$  ( $R^2 = 0.997$ , Figure 1h). The corresponding detection limit ( $3\sigma/\text{slope}$ ) for GSH was determined to be  $2.9 \times 10^{-8} \text{ M}$ . In addition, when these biological related species and NO coexisted in PBS buffer, only the combination of NO and GSH elicited a significant fluorescence intensity at  $595 \text{ nm}$ , implying that **1** can sequentially detect NO and GSH with high selectivity (Figure 1i). In addition, free **1** showed almost no fluorescence in the pH range of 4–9 but exhibited a strong fluorescence response for NO, which demonstrated that **1** displayed good suitability for the detection of NO at wide pH values ranging from 4 to 9 (Figure S8).

**Imaging of NO and GSH in HUVECs.** Encouraged by the above results in aqueous solutions, we continued to study its ability to monitor NO and GSH in human umbilical vein endothelial cells (HUVECs). Prior to bioimaging experiments, the cytotoxicity of **1** was evaluated by the CCK-8 assay. Probe **1** up to  $16 \mu\text{M}$  is nontoxic to HUVECs (Figure S9). Low cytotoxicity of **1** made it highly suitable for bioimaging. N-Ethylmaleimide (NEM, a GSH scavenger)-pretreated HUVECs subsequently incubated with **1** displayed weak fluorescence in both yellow and red channels (Figure 2a1–a3). Moreover, when we prolonged the incubation time from 0 to 60 min, weak fluorescence signals were observed in the red

channel, implying that the metabolism of NEM has a subtle impact on the upregulation of GSH in HUVECs (Figure S10). HUVECs pretreated with DEA-NONOate and then **1** exhibited remarkable fluorescence in both channels (Figure 2b1–b3). HUVECs directly incubated with **1** exhibited weak fluorescence at identical conditions, illustrating no reaction between **1** and intracellular GSH in the absence of NO (Figure 2c1–c3). When HUVECs were pretreated with NEM and DEA-NONOate and then loaded with **1**, an obvious fluorescence enhancement is observed only in the yellow channel (Figure 2d1–d3). Upon prolonging the incubation time, gradually increased fluorescence in the red channel was observed (Figure 2e), and the intensity ratio of the yellow to red channels decreased from 2.81 to 1.75 (Figure 2f), suggesting that exogenous NO stimulates the induction of GSH in HUVECs.

**Visualizing the NO-Induced GSH Upregulation Induced by Pravastatin or VC in HUVECs.** We further examined the interplay between NO and GSH in HUVECs in the presence of pravastatin (or VC). HUVECs incubated with **1** showed low fluorescence in both channels (Figure S11a1,a2). Fluorescence change was observed for pravastatin-pretreated HUVECs in the presence of **1** (Figure 3a). It increased gradually with the ratio (yellow/red) decreasing from 1.19 to 0.69 (Figure 3b,c). These results indicate the formation of **1**-NO followed by the transformation of **1**-NO to **1**-NO-GSH, which is due to the endogenous generation of NO and GSH in sequence. A marked decrease of fluorescence in the two channels was observed for pravastatin-pretreated HUVECs that were further incubated with L-NAME (a NOS inhibitor)<sup>43,44</sup> and **1** (Figure S11b1,b2). The result above proves that pravastatin is capable of increasing the NO level by activating NOS activity.  $\gamma$ -Glutamylcysteine synthetase ( $\gamma$ -GCS) is an essential enzyme for GSH synthesis.<sup>45</sup> For HUVECs loaded with pravastatin and further incubated with L-buthionine-sulfoximine (BSO, a  $\gamma$ -GCS inhibitor)<sup>46</sup> and **1**, a significant fluorescence decrease was observed in the red channel (Figure 3d) with the fluorescence ratio (yellow/red) decreasing from 2.39 to 1.51 (Figure 3e,f), demonstrating that the elevation of NO induces the augment of the GSH level through activating  $\gamma$ -GCS activity. Control experiments have been performed on HUVECs with the incubation of BSO and **1**. A negligible increase of fluorescence emission was observed

from 0 to 60 min, demonstrating that the BSO did not have an ability to influence GSH production (Figure S12). The above results confirmed that the GSH generation can mainly be attributed to  $\gamma$ -GCS upregulation activity induced by NO production in HUVECs in the presence of pravastatin. In addition, we continued to study how NO and GSH levels change in VC-treated HUVECs. Strong fluorescence emission in both two channels was displayed when HUVECs were treated with VC and then incubated with **1**. The ratio from the yellow to red channel decreased from 1.09 to 0.88 as the incubation time prolonged to 60 min (Figures S13b,c and S14). By contrast, cells treated with L-NAME, then VC, and **1** exhibited no fluorescence signal (Figure S13d). Meanwhile, the initial fluorescence in red channel was effectively quenched through the addition of BSO in VC-stimulated HUVECs containing **1**, and when we prolonged the incubation time from 0 to 60 min, fluorescence in the red channel was turned on gradually with the fluorescence ratio (yellow/red) decreasing from 1.98 to 1.57 (Figures S13e,f and S15). These results indicate that both pravastatin and VC can directly facilitate NO synthase (NOS) gene expression to elevate the level of NO. Then, the elevated NO concentration induces the activation of  $\gamma$ -GCS, leading to the augment of the GSH level *in vivo*. Thanks to the unique performance of probe **1** with sequential response toward NO and GSH, the NO-induced GSH upregulation in drug-treated HUVECs has been visualized for the first time.

**Imaging of NO and GSH in Zebrafish.** To explore the potential application of **1** *in vivo*, we employed it to monitor the changes of NO and GSH levels in zebrafish. Figures S16 and S17 manifest that **1** is tissue-permeable and capable of imaging exogenous NO and GSH in sequence in living bodies. We further investigated whether pravastatin could elicit NO and GSH formation sequentially in zebrafish. Low fluorescence was observed in the control zebrafish treated with **1** (Figure 4a1,a2), whereas zebrafish pretreated with pravastatin and then **1** displayed dramatic fluorescence in both channels (Figure 4b1,b2). The ratio of fluorescence intensity (yellow/red) is  $\sim 1$  (Figure 4e). For the control experiments, we incubated pravastatin-pretreated zebrafish with the L-NAME and **1**. Fluorescence was quenched in both channels (Figure 4c1,c2). Moreover, when zebrafish were pretreated with pravastatin and then loaded with BSO and **1**, significant fluorescence was displayed in the yellow channel, while weak fluorescence was displayed in the red channel (Figure 4d1,d2). The ratio (yellow/red) is  $\sim 2.8$  (Figure 4f). Similar results were obtained in VC-treated zebrafish (Figures S18 and S19). The above results indicated that probe **1** can be used for imaging sequential elevation of NO and GSH induced by pravastatin or VC in zebrafish.

## CONCLUSIONS

In summary, we synthesized a BODIPY-based fluorescence probe **1** for the exploration of the NO- and GSH-related signaling pathway during cardiovascular disease therapy. Probe **1** initially reacted with NO and showed a marked fluorescence enhancement, which further activated the reaction site toward GSH and led to red-shifted emission. The unique performance of probe **1** enabled sequential detection of NO and GSH, ensuring that it can only sense GSH increase induced by the prior presence of NO. More importantly, for the first time, we visualized the NO-induced GSH upregulation in pravastatin (or VC)-treated HUVECs and zebrafish using this probe,

demonstrating the connection between NO and GSH during the treatment. These results suggest that pravastatin or VC increases the level of endogenous NO through activating NOS, which downregulates the ROS concentration and improves the endothelial function effectively. Then, the endogenous NO can activate  $\gamma$ -GCS activity, resulting in a GSH increase (Scheme 1b). We expect this signaling pathway might have a guiding significance toward studying the pharmacological processes during cardiovascular disease therapy.

## ASSOCIATED CONTENT

### Supporting Information

The Supporting Information is available free of charge at <https://pubs.acs.org/doi/10.1021/acs.analchem.0c04754>.

Experimental synthesis, spectroscopic properties, cytotoxicity assay, fluorescence images, and characterization data (PDF)

## AUTHOR INFORMATION

### Corresponding Authors

**Li-Ya Niu** — Key Laboratory of Radiopharmaceuticals, Ministry of Education, College of Chemistry, Beijing Normal University, Beijing 100875, P. R. China;  [orcid.org/0000-0002-5376-6902](https://orcid.org/0000-0002-5376-6902); Email: [niuly@bnu.edu.cn](mailto:niuly@bnu.edu.cn)

**Qing-Zheng Yang** — Key Laboratory of Radiopharmaceuticals, Ministry of Education, College of Chemistry, Beijing Normal University, Beijing 100875, P. R. China;  [orcid.org/0000-0002-9131-4907](https://orcid.org/0000-0002-9131-4907); Email: [qzyang@bnu.edu.cn](mailto:qzyang@bnu.edu.cn)

### Author

**Xiao-Xiao Chen** — Key Laboratory of Radiopharmaceuticals, Ministry of Education, College of Chemistry, Beijing Normal University, Beijing 100875, P. R. China

Complete contact information is available at: <https://pubs.acs.org/10.1021/acs.analchem.0c04754>

### Notes

The authors declare no competing financial interest.

## ACKNOWLEDGMENTS

The authors thank Shihui Ding and Prof. Anming Meng for zebrafish embryos. This work was financially supported by the National Natural Science Foundation of China (21525206 and 21971023) to Q.-Z.Y.

## REFERENCES

- (1) Higashi, Y.; Noma, K.; Yoshizumi, M.; Kihara, Y. *Circ. J.* **2009**, 73, 411–418.
- (2) Ungvari, Z.; Tarantini, S.; Kiss, T.; Wren, J. D.; Giles, C. B.; Griffin, C. T.; Murfee, W. L.; Pacher, P.; Csiszar, A. *Nat. Rev. Cardiol.* **2018**, 15, 555–565.
- (3) Moellering, D.; McAndrew, J.; Patel, R. P.; Cornwell, T.; Lincoln, T.; Cao, X.; Messina, J. L.; Forman, H. J.; Jo, H.; Darley-Usmar, V. M. *Arch. Biochem. Biophys.* **1998**, 358, 74–82.
- (4) Lundberg, J. O.; Gladwin, M. T.; Weitzberg, E. *Nat. Rev. Drug Discovery* **2015**, 14, 623–641.
- (5) Espinosa-Díez, C.; Miguel, V.; Vallejo, S.; Sánchez, F. J.; Sandoval, E.; Blanco, E.; Cannata, P.; Peiró, C.; Sánchez-Ferrer, C. F.; Lamas, S. *Redox Biol.* **2018**, 14, 88–99.
- (6) Ongini, E.; Impagnatiello, F.; Bonazzi, A.; Guzzetta, M.; Govoni, M.; Monopoli, A.; Del Soldato, P.; Ignarro, L. J. *Proc. Natl. Acad. Sci. U.S.A.* **2004**, 101, 8497.
- (7) Yu, J.; Yao, H.; Gao, X.; Zhang, Z.; Wang, J.-F.; Xu, S.-W. *Biol. Trace Elem. Res.* **2015**, 163, 144–153.

- (8) Förstermann, U. *Nat. Clin. Pract. Cardiovasc. Med.* **2008**, *5*, 338–349.
- (9) Niu, L.-Y.; Chen, Y.-Z.; Zheng, H.-R.; Wu, L.-Z.; Tung, C.-H.; Yang, Q.-Z. *Chem. Soc. Rev.* **2015**, *44*, 6143–6160.
- (10) Wu, D.; Sedgwick, A. C.; Gunnlaugsson, T.; Akkaya, E. U.; Yoon, J.; James, T. D. *Chem. Soc. Rev.* **2017**, *46*, 7105–7123.
- (11) Kolanowski, J. L.; Liu, F.; New, E. *J. Chem. Soc. Rev.* **2018**, *47*, 195–208.
- (12) Zhang, J.; Chai, X.; He, X.-P.; Kim, H.-J.; Yoon, J.; Tian, H. *Chem. Soc. Rev.* **2019**, *48*, 683–722.
- (13) Park, S.-H.; Kwon, N.; Lee, J.-H.; Yoon, J.; Shin, I. *Chem. Soc. Rev.* **2020**, *49*, 143–179.
- (14) Yang, Y.; Zhao, Q.; Feng, W.; Li, F. *Chem. Rev.* **2013**, *113*, 192–270.
- (15) Sasaki, E.; Kojima, H.; Nishimatsu, H.; Urano, Y.; Kikuchi, K.; Hirata, Y.; Nagano, T. *J. Am. Chem. Soc.* **2005**, *127*, 3684–3685.
- (16) Lim, M. H.; Xu, D.; Lippard, S. *J. Nat. Chem. Biol.* **2006**, *2*, 375–380.
- (17) Lim, M. H.; Lippard, S. *J. Acc. Chem. Res.* **2007**, *40*, 41–51.
- (18) Wang, N.; Yu, X.; Zhang, K.; Mirkin, C. A.; Li, J. *J. Am. Chem. Soc.* **2017**, *139*, 12354–12357.
- (19) Reinhardt, C. J.; Zhou, E. Y.; Jorgensen, M. D.; Partipilo, G.; Chan, J. *J. Am. Chem. Soc.* **2018**, *140*, 1011–1018.
- (20) Teng, L.; Song, G.; Liu, Y.; Han, X.; Li, Z.; Wang, Y.; Huan, S.; Zhang, X.-B.; Tan, W. *J. Am. Chem. Soc.* **2019**, *141*, 13572–13581.
- (21) Huo, Y.; Miao, J.; Fang, J.; Shi, H.; Wang, J.; Guo, W. *Chem. Sci.* **2019**, *10*, 145–152.
- (22) Zhou, T.; Wang, J.; Xu, J.; Zheng, C.; Niu, Y.; Wang, C.; Xu, F.; Yuan, L.; Zhao, X.; Liang, L.; Xu, P. *Anal. Chem.* **2020**, *92*, 5064–5072.
- (23) Yang, M.; Fan, J.; Du, J.; Peng, X. *Chem. Sci.* **2020**, *11*, 5127–5141.
- (24) Chen, X.-X.; Niu, L.-Y.; Shao, N.; Yang, Q.-Z. *Anal. Chem.* **2019**, *91*, 4301–4306.
- (25) Niu, L.-Y.; Guan, Y.-S.; Chen, Y.-Z.; Wu, L.-Z.; Tung, C.-H.; Yang, Q.-Z. *J. Am. Chem. Soc.* **2012**, *134*, 18928–18931.
- (26) Umezawa, K.; Yoshida, M.; Kamiya, M.; Yamasoba, T.; Urano, Y. *Nat. Chem.* **2017**, *9*, 279–286.
- (27) Yin, C.-X.; Xiong, K.-M.; Huo, F.-J.; Salamanca, J. C.; Strongin, R. M. *Angew. Chem., Int. Ed.* **2017**, *56*, 13188–13198.
- (28) Qi, Y.; Huang, Y.; Li, B.; Zeng, F.; Wu, S. *Anal. Chem.* **2018**, *90*, 1014–1020.
- (29) Chen, J.; Wang, Z.; She, M.; Liu, M.; Zhao, Z.; Chen, X.; Liu, P.; Zhang, S.; Li, J. *ACS Appl. Mater. Interfaces* **2019**, *11*, 32605–32612.
- (30) Nie, L.; Gao, C.; Shen, T.; Jing, J.; Zhang, S.; Zhang, X. *Anal. Chem.* **2019**, *91*, 4451–4456.
- (31) Tian, X.; Li, Z.; Ding, N.; Zhang, J. *Chem. Commun.* **2020**, *56*, 3629–3632.
- (32) Malla, J. A.; Umesh, R. M.; Yousf, S.; Mane, S.; Sharma, S.; Lahiri, M.; Talukdar, P. *Angew. Chem., Int. Ed.* **2020**, *59*, 7944–7952.
- (33) Kang, Y.-F.; Niu, L.-Y.; Yang, Q.-Z. *Chin. Chem. Lett.* **2019**, *30*, 1791–1798.
- (34) Wang, F.; Zhou, L.; Zhao, C.; Wang, R.; Fei, Q.; Luo, S.; Guo, Z.; Tian, H.; Zhu, W.-H. *Chem. Sci.* **2015**, *6*, 2584–2589.
- (35) Zhang, R.; Zhao, J.; Han, G.; Liu, Z.; Liu, C.; Zhang, C.; Liu, B.; Jiang, C.; Liu, R.; Zhao, T.; Han, M.-Y.; Zhang, Z. *J. Am. Chem. Soc.* **2016**, *138*, 3769–3778.
- (36) Zhang, C.; Zhang, Q.-Z.; Zhang, K.; Li, L.-Y.; Pluth, M. D.; Yi, L.; Xi, Z. *Chem. Sci.* **2019**, *10*, 1945–1952.
- (37) Yue, Y.; Huo, F.; Cheng, F.; Zhu, X.; Mafireyi, T.; Strongin, R. M.; Yin, C. *Chem. Soc. Rev.* **2019**, *48*, 4155–4177.
- (38) Ou, P.; Zhang, R.; Liu, Z.; Tian, X.; Han, G.; Liu, B.; Hu, Z.; Zhang, Z. *Angew. Chem., Int. Ed.* **2019**, *58*, 2261–2265.
- (39) Li, H.; Shi, W.; Li, X.; Hu, Y.; Fang, Y.; Ma, H. *J. Am. Chem. Soc.* **2019**, *141*, 18301–18307.
- (40) Boens, N.; Leen, V.; Dehaen, W. *Chem. Soc. Rev.* **2012**, *41*, 1130–1172.
- (41) Niu, L.-Y.; Guan, Y.-S.; Chen, Y.-Z.; Wu, L.-Z.; Tung, C.-H.; Yang, Q.-Z. *Chem. Commun.* **2013**, *49*, 1294–1296.
- (42) Liu, X.-L.; Niu, L.-Y.; Chen, Y.-Z.; Yang, Y.; Yang, Q.-Z. *Biosens. Bioelectron.* **2017**, *90*, 403–409.
- (43) Schiattarella, G. G.; Altamirano, F.; Tong, D.; French, K. M.; Villalobos, E.; Kim, S. Y.; Luo, X.; Jiang, N.; May, H. I.; Wang, Z. V.; Hill, T. M.; Mammen, P. P. A.; Huang, J.; Lee, D. I.; Hahn, V. S.; Sharma, K.; Kass, D. A.; Lavandero, S.; Gillette, T. G.; Hill, J. A. *Nature* **2019**, *568*, 351–356.
- (44) Minato, H.; Hisatome, I.; Kurata, Y.; Notsu, T.; Nakasone, N.; Ninomiya, H.; Hamada, T.; Tomomori, T.; Okamura, A.; Miake, J.; Tsuneto, M.; Shirayoshi, Y.; Endo, R.; Otsuki, A.; Okada, F.; Inagaki, Y. *Hypertens. Res.* **2020**, *43*, 380–388.
- (45) Iida, T.; Kijima, H.; Urata, Y.; Goto, S.; Ihara, Y.; Oka, M.; Kohno, S.; Scanlon, K. J.; Kondo, T. *Cancer Gene Ther.* **2001**, *8*, 803–814.
- (46) Habermann, K. J.; Grünewald, L.; van Wijk, S.; Fulda, S. *Cell Death Dis.* **2017**, *8*, No. e3067.